Proc. Natl. Acad. Sci. USA
Vol. 94, pp. 6001–6006, June 1997
Applied Mathematics

Cilia internal mechanism and metachronal coordination as the result of hydrodynamical coupling

SHAY GUERON*†, KONSTANTIN LEVIT-GUREVICH*‡, NADAV LIRON*§, AND JACOB J. BLUM¶

*Department of Mathematics, Technion–Israel Institute of Technology, Haifa, 32000, Israel; and ¶Department of Cell Biology, Duke University Medical Center, Durham, NC 27710

Communicated by M. James Lighthill, University College London, London, United Kingdom, March 24, 1997 (received for review December 11, 1996)

ABSTRACT **We present a simple but realistic model for the internal bend-generating mechanism of cilia, using parameters obtained from the analysis of data of the beat of a single cilium, and incorporate it into a recently developed dynamical model. Comparing the results to experimental data for two-dimensional beats, we demonstrate that the model captures the essential features of the motion, including many properties that are not built in explicitly. The beat pattern and frequency change in response to increased viscosity and the presence of neighboring cilia in a realistic fashion. Using the model, we are able to investigate multicilia configurations such as rows of cilia and two-dimensional arrays of cilia. When two adjacent model cilia start beating at different phase, they synchronize within two cycles, as observed in experiments in which two flagella beating out of phase are brought close together. Examination of various multicilia configurations shows that metachronal patterns (i.e., beats with a constant phase difference between neighboring cilia) evolve autonomously. This provides modeling evidence in support of the conjecture that metachronism may occur as a self-organized phenomenon due to hydrodynamical interactions between the cilia.**

Ciliary motion and particularly the metachronism phenomenon have attracted a great deal of research effort both experimentally and theoretically. Metachronal coordination between cilia is a situation where cilia beat together with a constant phase difference between adjacent neighbors, their tips forming a moving wave pattern. The reason why arrays of cilia beat in a metachronal pattern is not fully understood. The work of Machemer (1), for example, shows that membrane voltage and calcium levels affect the direction of the metachronal wave and also the directions of the effective and recovery strokes of the ciliary beats. Some researchers speculate that the intriguing metachronism phenomenon is possibly the result of hydrodynamical coupling (e.g., see refs. 2–4). This work provides a theoretical model that supports this conjecture.

Gueron and Liron (ref. 5; GL hereafter) introduced an improved technique for describing the hydrodynamics of moving cilia, based on a refined slender body theory, which offers an alternative for the simplistic resistive force theory (known as the Gray and Hancock approximation) that relates drag forces and velocities. As a result, the accuracy and consistency of the model for cilia beating is markedly improved. More important, the GL equations provide a method for dynamical simulations of multicilia configurations that account for the effects of neighboring cilia and the effect of the surface from which the cilia emerge. This model was originally applied to a two-dimensional setup and later extended to describe three-dimensional beating (6).

The work of GL was mainly oriented toward developing the framework for dynamical modeling of multicilia configurations. For the internal mechanism of a cilium (hereafter referred to as the "engine") they used an *ad hoc* equation for the active (normal) shear force generated inside a cilium. However, the GL model has the engine as a separate building block which can be replaced (and is replaced here) by any other engine. For simplicity, the GL engine included a built-in frequency term that controls the resulting beat frequency and predetermines the duration of the effective and the recovery strokes. Therefore, this model does not allow for realistic changes in the beat frequency in response to external load such as increased viscosity or external flow generated by neighboring cilia. The GL engine cannot, therefore, be used for investigating metachronism. Murase (7) proposed an engine which is analogous in its form to muscle sliding models. However, his model is restricted to small-amplitude motion, which is not the case for real cilia, and is based on the Gray and Hancock approximation, which does not allow for modeling multicilia configurations. This engine gives poor results when incorporated into the GL model.

We present a simple plausible functional form for the engine that is related to the dyenin arms and the radial spokes system (see refs. 8 and 9). This engine has a small number of parameters. To obtain realistic values for the parameters we use observations of ciliary motion to compute locations and velocities during the beat cycle, solve the GL equations to compute the drag forces, and then compute the internal shear forces. These forces are then used to determine the engine parameters. The computed engine is tested by incorporating it into the GL dynamical equations for two-dimensional beats. The model produces realistic beats, and it reproduces experimental results such as exponential decrease in beat frequency with increased viscosity, self-synchronization between two adjacent cilia, and frequency matching with the frequency of external flows. Finally, we investigate multicilia configurations and find that metachronal patterns evolve autonomously due to the hydrodynamical interaction between the cilia. This supports the conjecture that metachronism can be explained as the result of hydrodynamical coupling.

The Model Equations

The drag–velocity relation, combined with the two-dimensional curve geometry, yields the following three integro partial differential equations, written in nondimensional form (see ref. 5):

The publication costs of this article were defrayed in part by page charge payment. This article must therefore be hereby marked "*advertisement*" in accordance with 18 U.S.C. §1734 solely to indicate this fact.

Abbreviation: GL, Gueron and Liron.

†e-mail: shay@math.technion.ac.il.
‡e-mail: konstant@math.technion.ac.il.
§e-mail: liron@math.technion.ac.il.

$$F_N = \frac{E_b}{S_0 L^2}\alpha_{ss} + S, \quad [1]$$

$$F_{T_{ss}} = (1 + C_{TN})F_{N_s}\alpha_s + C_{TN}F_T(\alpha_s)^2 + F_N\alpha_{ss} - C_{TN}g_N\alpha_s + g_{T_s}, \quad [2]$$

$$F_{N_{ss}} + (1 + C_{NT})F_{T_s}\alpha_s + F_T\alpha_{ss} = -(C_N\omega L^2/S_0)\alpha_t + C_{NT}F_N(\alpha_s)^2 + C_{NT}g_T\alpha_s + g_{N_s}. \quad [3]$$

We use boundary conditions that correspond to a cilium that is pinned at its basal end and free at its distal end, and initial conditions that correspond to an erect cilium:

$$\alpha_s(0, t) = 0, \quad \alpha_{sss}(0, t) = -\frac{S_0 L^2}{E_b} S_s(0, t),$$

$$\alpha_s(1, t) = 0, \quad \alpha_{ss}(1, t) = -\frac{S_0 L^2}{E_b} S(1, t),$$

$$F_{T_s}(0, t) = F_{N_s}(0, t) = 0, \quad F_N(1, t) = F_T(1, t) = 0,$$

$$\alpha(s, 0) = \frac{\pi}{2}. \quad [4]$$

In Eqs. **1–4** s is the arclength variable of the centerline of the cilium, measured from the basal end, t is time, and the functions depend on s and t (we omit writing this dependence explicitly when it is clear from the context). The subscripts s and t denote the space and time derivatives, respectively. The function $\alpha = \alpha(s, t)$ measures the angle between the tangent to the cilium and the horizontal axis. α is related to $\kappa = \kappa(s, t)$, the curvature of the cilium's centerline, by the equation $\kappa = \alpha_s$. F_N and F_T are the normal and tangential components of the shear force generated inside the cilium, respectively. $S = S(s, t)$ is the active shear force due to the internal sliding filaments mechanism and the radial spokes system. The model equation representing S is derived below. S_0 is a typical fixed magnitude of the internal shear force (used for scaling), L is the length of the cilium, and E_b is its elastic bending resistance. The expressions g_T, g_N involve integrals of the appropriate singular solutions of Stokes flow, C_N and C_T are the related GL coefficients, $C_{TN} = C_T/C_N$, and $C_{NT} = C_N/C_T$. These equations, derived in detail by GL, are outlined in the *Appendix*.‖

Because we deal here with a two-dimensional problem, the angle (α) determines the centerline curve if the position and the orientation at $s = 0$ (i.e., the anchor of the cilium) are given.

The normal shear force F_N in Eq. **1** includes the contribution due to the elastic resistance of the cilium and the active shear force $S(s, t)$. Clearly, $S(s, t)$ determines the dynamics of the cilium in the following way: If the position of the cilium (α) is given at time t, one can calculate F_N from Eq. **1**. F_T can then be obtained from Eq. **2**, which relates the normal and the tangential components of the shear force (due to the inextensibility of the cilium). α is propagated in time by means of Eq. **3**.

A Load-Dependent Internal Engine

In this section we briefly describe our method for modeling the internal mechanism of cilia. As data, we use the observed (two-dimensional) beat pattern of the cilium of *Paramecium* (diagrams and discussion in refs. 10 and 11). We measure the coordinates of equally spaced points along the cilium at different times during the beat cycle. The velocity of the cilium is calculated from these data (after proper smoothing). Using the calculated velocity, we solve the integral Eqs. **1–3** for the drag forces as unknowns, and then compute the active shear force $S(s, t)$.

According to Sleigh and Barlow (9), the radial spokes system contributes to the total shear force at the bent region but not at the straight region. A reasonable intrinsic (and local) indicator of the place of the bend is the curvature $\kappa(s, t) = \alpha_s(s, t)$. Therefore, we fit the *measured* function $S(s, t)$ to a simple combination of functions of the curvature, the arclength s and the deviation from the resting position:

$$S(s, t) = (\pm 1) \cdot \left\{ \bar{C}_N\omega \frac{(s^2 - 1)}{2} \cdot \left[1 + \left(A_1 + A_2\left(\alpha(0, t) - \frac{\pi}{2} \right)^2 \right) \right] + B\cdot\kappa(s, t) \right\}. \quad [5]$$

Here, ω (a typical angular velocity), $\bar{C}_N = C_N L^2/S_0$, and A_1, A_2 are parameters used for scaling. ω, A_1, A_2 have different values during the effective and the recovery strokes. To simulate the fast initiation of the bend at the beginning of the recovery stroke, we take A_1 in the region $0 \le s < 0.1$ to be twice as large as its value in the region $0.1 \le s \le 1$. Altogether, the effective stroke is determined by four parameters ($\bar{C}_N\omega$, A_1, A_2, B) and the recovery stroke by five (A_1 has two values). Note that $\bar{C}_N$ and ω appear only as the product $\bar{C}_N\omega$ but are artificially separated to introduce a realistic frequency term (ω) and for consistency with the model equations developed by GL.

The first term in Eq. **5** represents the contribution of the dynein arms, and the second curvature-dependent term represents the contribution of shear-resistant elements such as the radial spokes and nexins. Note that during the effective stroke the cilium is almost straight ($\kappa \sim 0$), and thus only the dynein arms contribute to the motion.

Our engine has a similar functional form during the effective and the recovery stroke but with opposite signs (+ during the effective stroke and − during the recovery stroke). This is based on the evidence (10) that different groups of filaments are active at different stages of the beat cycle. To complete the definition of the model we must specify when the switching between the two phases of the motion occurs.

We speculate that the effective stroke continues as long as the filaments can slide in this direction, that is, until the effective shear σ between filaments reaches a certain maximal value (note that the effective shear is a geometric quantity, not to be confused with the active shear force. For details see ref. 8. Since the cilium is inextensible, we have $\partial\sigma/\partial s = \partial\alpha/\partial s$, which implies $\sigma(s, t) = \alpha(s, t) + [\sigma(0, t) - \alpha(0, t)]$. It follows that during the effective stroke σ corresponds directly to the inclination angle of the cilium. Therefore, the criterion we choose for the switching between the effective and the recovery strokes is reaching a maximal inclination angle (denoted α_{right}) at the basal region.

During the recovery stroke, the maximal effective shear is attained when the cilium completes its straightening process. The criterion we choose for the switching between the recovery and the effective strokes is, therefore, returning to an erect position.

It is important to note that Eq. **5** represents a load (geometry)-dependent engine, since the beat pattern and the frequency depend on the environment. External flow (e.g., due to neighboring cilia) and external load (e.g., changes in the viscosity of the surrounding fluid) affect $\alpha(s, t)$. Because the engine depends on the geometry and the switching depends on

‖The values used in the model are $S_0 = 10^{-12}$ N, $L = 12$ μm, $E_b = 25\cdot10^{-24}$ N·m^2, $C_N = 0.0035$ kg/m·s, and $C_T = 0.0025$ kg/m·s.

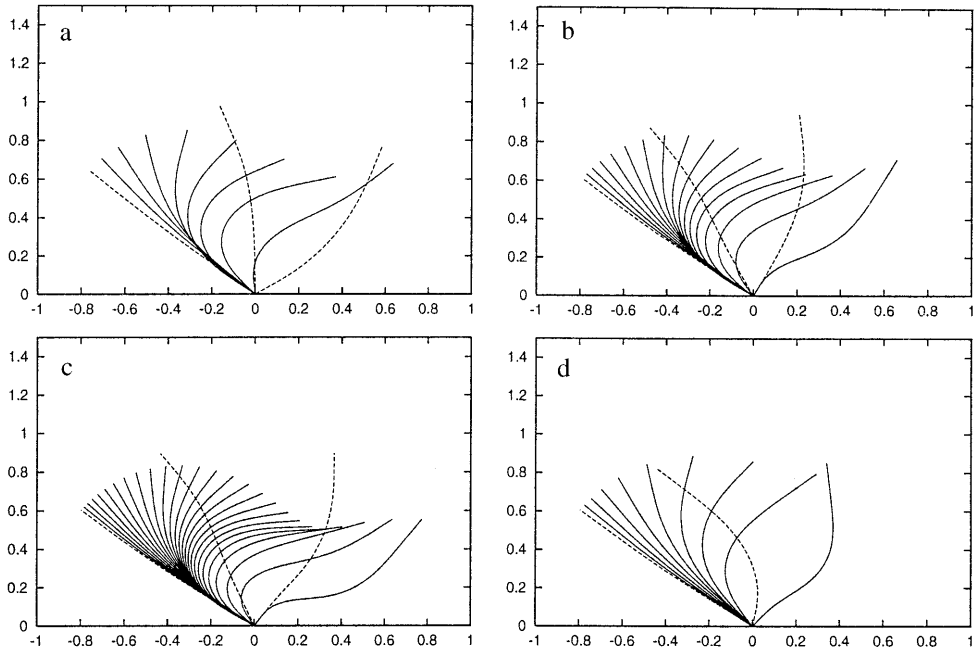

FIG. 1. Beat cycles of cilia. All positions are equally separated in time by 3 ms. The effective stroke positions are plotted by dashed lines, and the recovery stroke positions by solid lines. The units of the axes are nondimensional length. (*a*) A single cilium. The viscosity of the surrounding fluid is that of water, $\mu = \mu_{\text{water}}$. The resulting beat frequency is ≈29 Hz. (*b*) $\mu = 2\mu_{\text{water}}$. The resulting beat frequency is ≈17 Hz and the beat pattern is changed. (*c*) $\mu = 3\mu_{\text{water}}$. The resulting beat frequency is ≈12 Hz and the beat pattern is changed. (*d*) Side view of an infinite line of synchronized cilia, spaced by 0.3 ciliary length, beating in water. The resulting beat frequency is ≈29 Hz.

reaching some "final position," changes in $\alpha(s, t)$ affect the beat frequency as well.

The parameter values used in our model are $\omega_{\text{eff}} = 11{,}000°/\text{s}$, $\omega_{\text{rec}} = 2{,}290°/\text{s}$, $\alpha_{\text{left}} = 130°$ and $\alpha_{\text{right}} = 20°$. These are measured directly from data (beat cycles from ref. 10). During the effective stroke $A_1 = 0.26$ and $A_2 = -0.17$, and during the recovery stroke $A_1 = 2$ for $0 \le s \le 0.1L$ and $A_1 = 1$ for $0.1L \le s \le L$, $A_2 = -2$, and $B_{\text{eff}} = 0$ and $B_{\text{rec}} = 2$. These parameters were obtained by fitting the measured data.

Results

Fig. 1*a* displays snapshots of the beat cycle of a single cilium, having an engine described by Eq. **5** and dynamics computed by Eqs. **1–3**. Clearly, the model produces a realistic beat pattern: during the effective stroke (dashed lines), the cilium moves almost as a straight rod, and during the recovery stroke (solid lines) a bend is generated at the basal end and propagates toward the distal end. Table 1 compares the model results to experimental data, demonstrating that the model cilium captures all essential features of the motion.

Table 1. Comparison between the properties of the model cilia and experimental data

Parameter	Dimensions	Data*	Model
Beat duration	ms	35.7	≈34
Beat frequency	cycles/s	28	≈29.4
Angular range of the effective stroke	°	110	110–115
Duration of the effective stroke	ms	≈9	≈7–8
Duration of the recovery stroke	ms	≈26	≈26
Ratio of durations (recovery/effective)		2.9	3.25
Duration of basal swing during the recovery stroke	ms	6	≈7

*See ref. 10.

Machemer (1) observed that the beat frequency of the cilia of *Paramecium* decreases approximately linearly when plotted against the logarithm of viscosity. Brokaw (12) investigated this dependence with various types of flagella and found the same behavior. In the present model, both beat pattern and frequency change with increasing viscous load. In Fig. 2 we plot the calculated beat frequency as a function of the viscosity in the range $\mu_{\text{water}} \le \mu \le 5\mu_{\text{water}}$, reproducing a linear dependence. Since this dependence is not explicitly assumed in the model, this suggests that the fundamental characteristics of the ciliary motility are captured by the present model. The ciliary beat frequencies (shown in Fig. 2) measured by Machemer in the range $\mu_{\text{water}} \le \mu \le 5\mu_{\text{water}}$ for a multicilia configuration in *Paramecium* are higher than what we obtain for the single isolated model cilium, but the slopes of the resulting lines are roughly similar. This difference is consistent

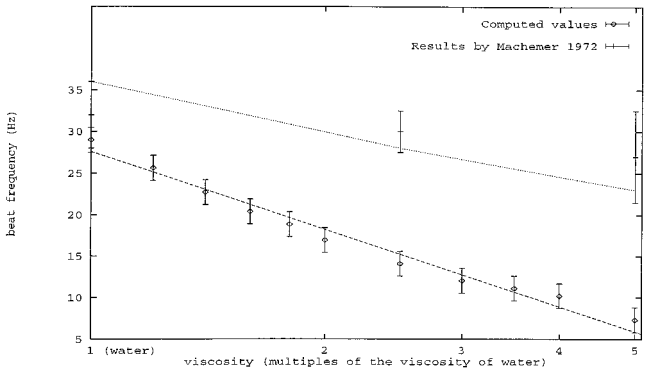

FIG. 2. Dependence of the beat frequency on the viscosity, for a single cilium, in the range $\mu_{\text{water}} \le \mu \le 5\mu_{\text{water}}$. The vertical error bars represent model results with the estimated measurement errors, and the dashed line is a minimal least-squares fit. The linear decrease in beat frequency with exponentially increasing viscosity for the cilia of *Paramecium*, shown in the figure, is reproduced from ref. 1. Note that the abscissa is on a logarithmic scale.

with our results for multicilia configurations. As reported below, the beat frequency of the model cilia indeed increases in the presence of neighboring cilia. Note that since the cilia of *Paramecium* change the plane of beating when the viscosity is increased by more than about 5-fold that of water (see ref. 1) and the present model does not include this possibility, we do not study the behavior of the model cilia outside this range.

To check the sensitivity of our model engine to external load, we subjected the model cilia to an external periodic flow, parallel to the cell's surface and satisfying the no-slip boundary condition. In the range from 29 to 55 Hz the cilium tends to match its beat frequency to the frequency of the external flow (data not shown).

Cilia interactions is another important aspect we study. When neighboring cilia beat close enough to each other, each one is subjected to the flow generated by the others. This influences their beat pattern and beat frequency. The model results indicate that the influence is negligible if the distance between the cilia exceeds two cilium lengths.

The simplest/smallest multicilia configuration consists of two cilia. Gray (13) reported on experiments with two flagella, beating initially at different frequencies and having different wavelengths. When these are put close enough to each other, they tend to quickly synchronize, and beat with the same frequency and in phase. An analogous phenomenon of self-synchronization and phase locking between rings and lines of coupled oscillators is well known. It was investigated experimentally and theoretically (e.g., for one-dimensional weakly coupled chains and rings of oscillators, see refs. 14 and 15), but here we have a complex realistic biological system. Fig. 3 displays snapshots of the beat cycles of two cilia separated by one cilium length, beginning their beat at opposite phases. As shown in the figure, they synchronize completely within two cycles. The final mutual beat frequency increases slightly from 29.5 Hz (for a single cilium) to 31 Hz. This is an indication of the "advantage" of some multicilia configurations. The presence of neighboring cilia (one in this case) "helps" them beat faster.

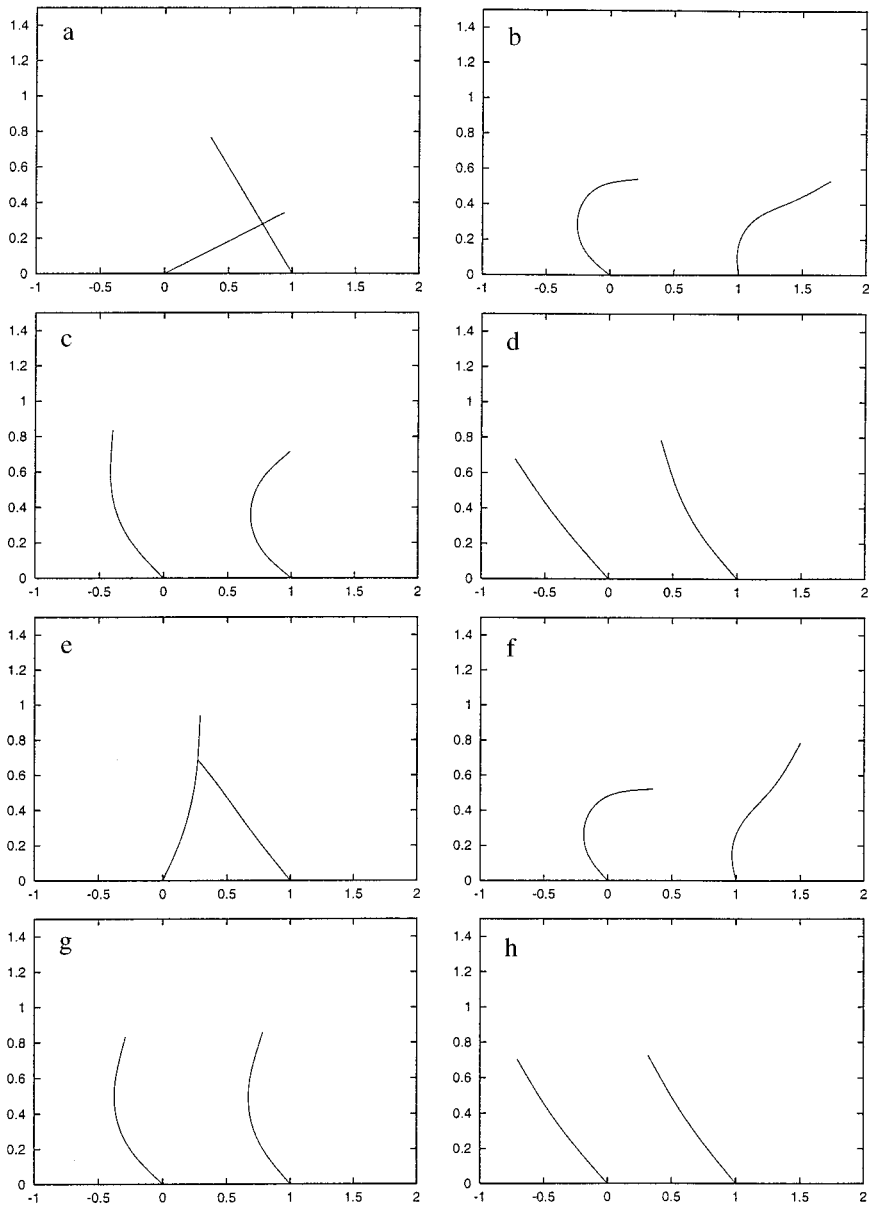

FIG. 3. Autonomous synchronization between two cilia starting at opposite phases (the left cilium starts at the recovery stroke and the right cilium starts at the effective stroke). Synchronization is achieved after two cycles. Cilia spacing is 1. The snapshots, labeled successively from *a* to *h*, are separated in time by 9 ms. The resulting beat frequency is ≈31 Hz. The units of the axes are nondimensional length.

Metachronal coordination is characteristic of ciliary arrays. The cilia on same line (perpendicular to the direction of the effective stroke) are synchronized, and adjacent rows of cilia (parallel to the direction of the effective stroke) beat with a phase difference. Antiplectic metachronism is a situation in which the metachronal wave (defined by the tips of the beating cilia) propagates in a direction opposite to the direction of the effective stroke (e.g., in *Paramecium*, see refs. 1 and 10). In such configurations, each individual cilium is influenced by cilia located on the same line as well as by cilia located on neighboring rows. To ascertain whether the model would generate self-organized metachronism, we used multicilia configurations where the cilia start simultaneously with the same initial conditions. Fig. 4 displays snapshots of 10 cilia and a 100 cilia configurations. Both cases develop antiplectic metachronal waves, which is typical for the cilia of *Paramecium*. The beat frequency does not change significantly when the number of cilia exceeds 10 (42 Hz). This is because, as mentioned above, the spatial range of the interaction is limited. The cilia reach their steady-state beat patterns after a few cycles, and the results shown in Fig. 4 are already at steady state.

Liron (16) developed an efficient method for calculating the velocity induced at a point by an infinite line of Stokeslets, located at a fixed height above a flat surface (see also ref. 17). Changing the expression for g_N and g_T in Eqs. **1–3** to include the appropriate kernels (16) enables us to model the dynamics of an infinite line of synchronized cilia (the beat remains planar) and two-dimensional arrays consisting of several rows each representing an infinite line of synchronized cilia. Fig. 1*d* shows the side view of an infinite line of synchronized cilia. It is interesting to observe that, although the beat pattern is changed compared with a single cilium (compare Fig. 1*d* with *a*), the resulting frequency (≈29 Hz) remains almost unchanged, unlike the case for a row of cilia. As for the single-row configuration, metachronal phase differences emerge from the dynamics due to the hydrodynamical interactions.

This paper describes a framework for modeling the internal mechanism of cilia, which can be used for various cases based

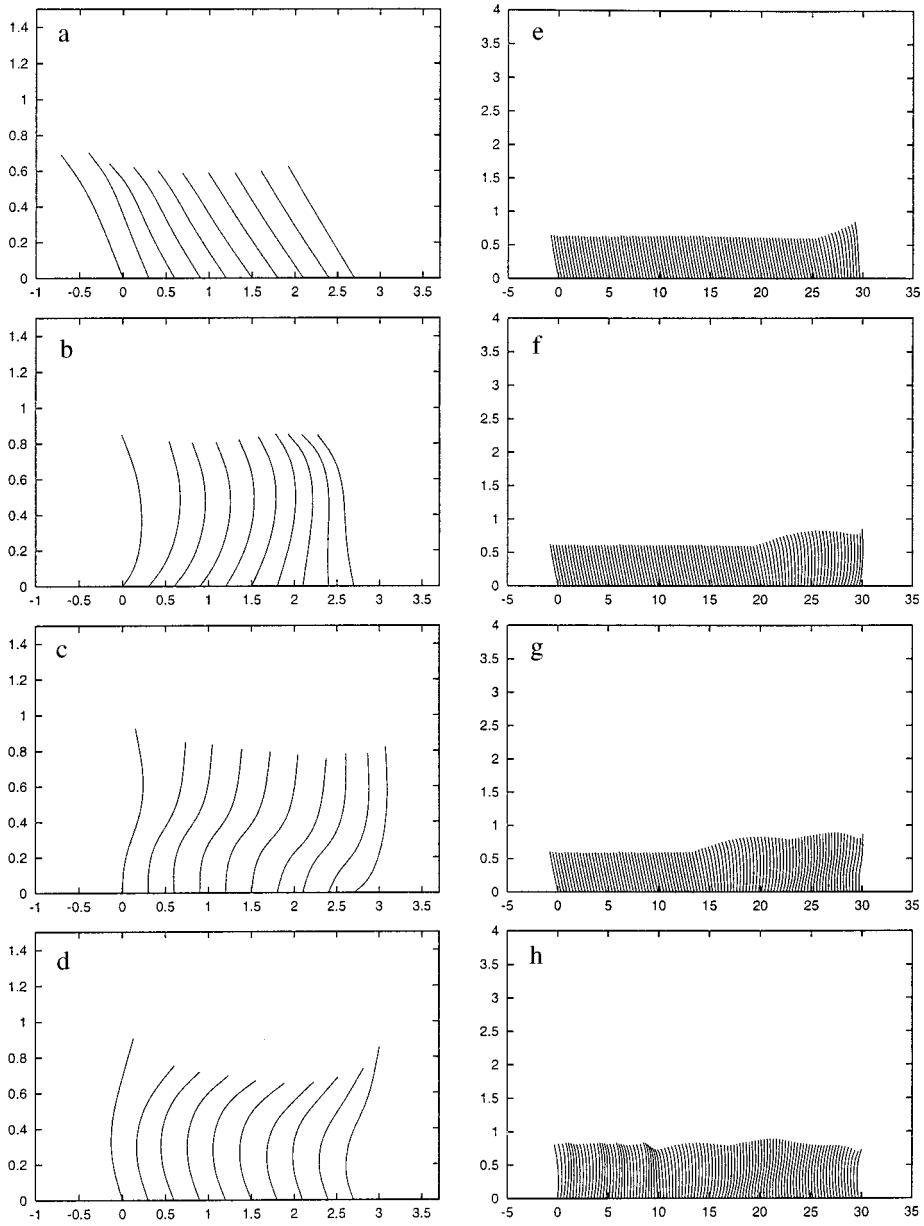

FIG. 4. (*a–d*) Self-organized metachronism in a row of 10 cilia. (*e–f*) Metachronism in the 100-cilia configuration. Metachronal wave pattern is generated by hydrodynamical coupling. In both configurations the cilia spacing is 0.3, the snapshots are separated in time by 2 ms, the resulting beat frequency is ≈42 Hz, and the units of the axes are nondimensional length.

on experimental data. We used this approach successfully with data for *Paramecium*. Our results demonstrate that for closely packed ciliary arrays such as those found on ciliates, hydrodynamic interactions between neighboring cilia are sufficient to account for antiplectic metachrony. In principle, it is also possible to use our approach with appropriate data to investigate the formation of symplectic metachrony. Whether hydrodynamic effects alone are sufficient to cause diaplectic metachronal waves requires extension of the present model to include an ''engine'' that generates a realistic three-dimensional beat. Such studies have been initiated. It should also be pointed out and that in airways, where the tips of the cilia penetrate into the lower surface of a thin layer of mucus during the effective stroke, hydrodynamic interactions between neighboring cilia may be insufficient by themselves to generate metachronal wave propagation. The properties of the mucus would need to be included in a suitable theoretical model.

Appendix

The integral expressions for g_N and g_T, as derived by G.L. (5), are:

$$g_N = C_N G_N, \quad g_T = C_T G_T, \qquad \textbf{[6]}$$

where G_N and G_T are the normal and tangential components of the vector **G**.

$$\begin{aligned}\mathbf{G}(s_0, t) = &\int_{|s-s_0|>q} \mathbf{U}_s(r(s_0, t), r(s, t), -\phi(s, t))ds + \\ &\int_{0\le s\le L} \{\mathbf{V}_{si}(r(s_0, t), r(s, t), -\phi(s, t)) + \\ &\int_{0\le s\le L} \{\mathbf{V}_{si}(r(s_0, t), r(s, t), -\phi(s, t)) + \\ &\qquad \mathbf{V}_{di}(r(s_0, t), r(s, t), -(a^2/4\mu)\phi(s, t))\} + \\ &\int_{\substack{0\le s\le L \\ \text{neighboring cilia}}} \mathbf{U}_s(r(s_0, t), r(s, t), -\phi(s, t))ds \qquad \textbf{[7]}\end{aligned}$$

and

$$C_T = \frac{8\pi\mu}{-2 + 4\ln(2q/a)}, \quad C_N = \frac{8\pi\mu}{1 + 2\ln(2q/a)}. \qquad \textbf{[8]}$$

We use $q = 1$ μm (the parameter that determines the integration limits) and $a = 0.1$ μm (the radius of the cilium) as in ref. 5.

Here, $\mathbf{U}_s(r, r_0, \phi)$ is the velocity induced at r by a Stokeslet with intensity ϕ, located at r_0. $\mathbf{U}_{si}(r, r_0, \phi)$ is the velocity induced at r by a Stokeslet located at r_0, with intensity ϕ, and by its image system. $\mathbf{U}_d(r, r_0, \phi)$ is the velocity induced at r by a doublet with intensity ϕ, located at r_0. $\mathbf{U}_{di}(r, r_0, \phi)$ is the velocity induced at r by a doublet located at r_0, with intensity ϕ, and by its image system. $\mathbf{V}_{si}(r, r_0, \phi) = \mathbf{U}_{si}(r, r_0, \phi) - \mathbf{U}_s(r, r_0, \phi)$. $\mathbf{V}_{di}(r, r_0, \phi) = \mathbf{U}_{di}(r, r_0, \phi) - \mathbf{U}_d(r, r_0, \phi)$. Eq. **7** with the coefficients in **8** is an approximation up to the order $O(\sqrt{\varepsilon})$, where $\varepsilon = a/L$ measures the cilium's slenderness (1/120 in our case). Details are given by G.L. (5).

This research was supported by the U.S.–Israel Binational Science Foundation (Grant 94-242), by the Technion Vice President for Research Fund, and by the Fund for the Promotion of Research at the Technion. S.G. acknowledges the support of the Henri Gutwirth Fund for the Promotion of Research. K.L.-G. acknowledges the support of the Technion Graduate School.

1. Machemer, H. (1972) *J. Exp. Biol.* **57,** 239–259.
2. Sleigh, M. A. (1969) *Int. Rev. Cytol.* **25,** 31–54.
3. Sleigh, M. A., ed. (1974) *Cilia and Flagella* (Academic, London).
4. Gheber, L. & Priel, Z. (1989) *Biophys. J.* **55,** 183–191.
5. Gueron, S. & Liron, N. (1992) *Biophys. J.* **63,** 1045–1058.
6. Gueron, S. & Liron, N. (1993) *Biophys. J.* **65,** 499–507.
7. Murase, M. (1990) *J. Theor. Biol.* **146,** 209–231.
8. Hines, M. & Blum, J. J. (1978) *Biophys. J.* **23,** 41–57.
9. Sleigh, M. A. & Barlow, D. I. (1982) *Symp. Soc. Exp. Biol.* **35,** 139–157.
10. Sleigh, M. A. (1962) *The Biology of Cilia and Flagella* (Pergamon, Oxford).
11. Sleigh, M. A. (1968) *Symp. Soc. Exp. Biol.* **22,** 131–150.
12. Brokaw, C. J. (1966) *J. Exp. Biol.* **45,** 113–139.
13. Gray, J. (1928) *Ciliary Movement* (Cambridge Univ. Press, Cambridge, U.K.).
14. Ermentrout, G. B. & Kopell, N. (1984) *SIAM J. Math. Anal.* **15,** 215–237.
15. Ermentrout, G. B. (1985) *J. Math. Biol.* **23,** 55–74.
16. Liron, N. (1996) *J. Eng. Math.* **30,** 267–297.
17. Liron, N. & Mochon, S. (1976) *J. Fluid Mech.* **75,** 593–607.